Journal of the Meteorological Society of Japan

EARLY ONLINE RELEASE

This is a PDF of a manuscript that has been peer-reviewed and accepted for publication. As the article has not yet been formatted, copy edited or proofread, the final published version may be different from the early online release.

This pre-publication manuscript may be downloaded, distributed and used under the provisions of the Creative Commons Attribution 4.0 International (CC BY 4.0) license. It may be cited using the DOI below.

The DOI for this manuscript is
DOI:10.2151/jmsj.2020-064
J-STAGE Advance published date: August 28th, 2020
The final manuscript after publication will replace the preliminary version at the above DOI once it is available.

Multiyear La Niña impact on summer temperature over Japan

Tomoki IWAKIRI[1]

and

Masahiro WATANABE

Atmosphere and Ocean Research Institute

The University of Tokyo, Tokyo, Japan

August 3, 2020

----

1) Corresponding author:

T. Iwakiri, Atmosphere and Ocean Research Institute, The University of Tokyo

5-1-5 Kashiwanoha, Kashiwa, Chiba 277-8568, Japan

Email: iwakiri@aori.u-tokyo.ac.jp

Abstract

La Niña is the negative phase of the El Niño-Southern Oscillation (ENSO) cycle. It occurs in the equatorial Pacific, and events known as multiyear La Niña often persist for more than two years. During a conventional La Niña event, the seasonal cycle of surface temperature over Japan is known to be amplified (i.e. hotter summer and colder winter than normal years), but the influence of multiyear events on temperature over Japan has not yet been clarified. In this study, we evaluate the teleconnection associated with multiyear La Niña using composite analyses of observations, reanalysis data, and a large-ensemble of atmospheric general circulation model (AGCM) simulations for 1951–2010 driven by observed boundary conditions, and propose two distinct mechanisms involved in multiyear La Niña causing hot summers over Japan.

Composites of observational data show significant positive temperature anomalies over Japan in the boreal summer season preceding the two consecutive La Niña events reaching their mature phases. This robust summer signal can be reproduced by AGCM large ensemble simulations, which indicates that it is forced by multiyear La Niña. The time evolution of the anomalous summer temperature over Japan differs between the first and second years of multiyear La Niña. In the first summer, warm conditions are found in August–

October in the southwestern part of Japan, due to anomalous southwesterly winds in the lower troposphere. This atmospheric circulation anomaly can be explained by a La Niña-induced decrease in precipitation over the equatorial western Pacific. In the second summer, warm anomalies are found in June–August over northeastern Japan, and these are accompanied by an anomalous barotropic high-pressure induced by negative precipitation anomalies over the equatorial Pacific. The seasonal march in atmospheric background states and the delayed effect of a preceding El Niño may explain the distinct teleconnection during multiyear La Niña.

Keywords ENSO teleconnection; multiyear La Niña; hot summer

1. Introduction

The El Niño-Southern Oscillation (ENSO) is the most dominant air–sea coupled variability in the climate system. The sea surface temperature (SST) in the eastern equatorial Pacific is higher than the climatological mean during a conventional El Niño, and the contrary occurs during La Niña. The ENSO temporal evolution is known to be seasonally locked (Jin et al. 1994; Tziperman et al. 1994): El Niño and La Niña develop in boreal summer, peak in winter, and decay in the following spring. In addition, anomalous SSTs modulate equatorial convective activities that cause extreme weather events throughout the world via atmospheric teleconnection patterns (Lau 1997; Trenberth et al. 1998; Trenberth 2002).

One of the well-known ENSO teleconnection is the Pacific/North American (PNA) pattern during winter (Wallace and Gutzler 1981; Horel and Wallace 1981). The positive phase of the PNA pattern is frequently observed during the El Niño winter, and it consists of negative geopotential height anomalies over the North Pacific and positive anomalies over North America. ENSO teleconnections occur not only during the peak phase of El Niño but also during its development and decay phases and throughout the following seasons. For example, when El Niño

SST signals have diminished in the equatorial Pacific, the tropospheric temperature remains warm (Yulaeva and Wallace 1994; Sobel et al. 2002; Chiang and Sobel 2002); This is partly due to basin-wide warming in the Indian Ocean during spring and summer and is often explained as a tropical atmospheric bridge (Klein et al. 1999; Schott et al. 2009). The Indian Ocean acts as a heat capacitor, and the delayed warming therein affects the atmospheric circulation over surrounding regions (Xie et al. 2009). Although the anomalous convective activity over the equatorial Pacific is not perfectly symmetrical between El Niño and La Niña, a similar remote influence can be seen during La Niña because the atmospheric circulation anomaly can be well understood based on linear Rossby wave theory (Hoskins and Karoly 1981).

Recent studies have reported another remarkable difference between El Niño and La Niña; the latter often occurs in two consecutive years and is known as a multiyear (alternatively double-dip, follow-up, or two-year) La Niña (Hu et al. 2014; DiNezio and Deser 2014; Luo et al. 2017; DiNezio et al. 2017a,b). ENSO is believed to be a quasi-periodic linear oscillation (Battisti and Hirst 1989; Jin 1997), and multiyear La Niña cannot be explained by the linear ENSO theory. It has been suggested that multiyear La Niña arises from a nonlinearity in the atmospheric response to SST anomalies or nonlinear dynamical processes associated with the thermocline displacement (Okumura and Deser 2010; DiNezio and Deser 2014; An and Kim 2018); However, the mechanism involved in multiyear La Niña has not yet been clarified.

Multiyear La Niña may result in teleconnections that are different to those of conventional La Niña. For example, during the peak of the second La Niña, severe drought occurred in the United States of America through zonally prolonged PNA pattern, despite the negative SST anomalies being weaker than those of the first year (Okumura et al. 2017). Although past studies have identified the impacts of multiyear La Niña on weather conditions over several regions, no study has investigated the influence of multiyear La Niña on the weather and climate over Japan to date. There is a possible existence of a different teleconnection mechanism exerted by multiyear La Niña compared to that of the conventional La Niña, which brings hot summers and cold winters (Kurihara 1985; Kitoh 1988; Miyazaki 1989; Tanaka et al. 2015).

In this study, we evaluate the impacts of multiyear La Niña on the temperature over Japan by analyzing observational data and large ensemble simulations from an atmospheric general circulation model (AGCM) driven by observed SST, sea ice, and radiative forcing. The remainder of this paper is presented as follows: the data and methodology are described in Section 2, composite analysis results of surface temperature over Japan are presented in Section 3, large scale analyses are conducted in Section 4 to identify teleconnection differences between the first and second years of multiyear La Niña, Section 5 explores the dynamic mechanisms relating to the teleconnection, and Section 6 presents a summary and discussion.

2. Data and methods

2.1. Observations and reanalysis data

We used instrumental measurements of monthly mean surface air temperature (SAT) for 1901–2017 at 13 stations over Japan (Nemuro, Suttu, Yamagata, Ishinomaki, Fushiki, Choshi, Sakai, Hamada, Hikone, Tadotsu, Nase and Ishigakijima). The observation systems are maintained by the Japan Meteorological Agency (JMA; cf. JMA 2017) and are located outside of mega cities where they are least affected by the heat island effect. The average data obtained at these stations were used as a reference for SAT observations over Japan. Furthermore, sectorial mean SATs for four areas (northern, western, southern, and eastern Japan) are available for a shorter period of 1951–2010. To define La Niña events, we used observed monthly SST data for 1901–2017 derived from COBE-SST2 (Hirahara et al. 2014). We also used monthly precipitation data from the National Oceanic and Atmospheric Administration (NOAA) Precipitation Reconstruction (PREC) for 1951–2010 (Chen et al. 2002).

We used four reanalysis data sets as global atmospheric data: CERA-20C (1901–2010, Laloyaux et al. 2018), NOAA-20CR (1901–2010, Compo et al. 2006), ERA-20C (1901–2010, Poli et al. 2016), and NCEP/NCAR Reanalysis 1 (1951–2018, Kalnay et al. 1996). CERA-20C is the latest reanalysis data set; it is based on a coupled atmosphere–ocean model and consists of ten ensemble members representing observational uncertainty. We analyzed each of the four data sets; the results were found to be very similar, and thus present the results based on the ensemble mean of CERA-20C. To match the period of large-ensemble simulations (Section 2.2), the analysis period of 1951–2010 was selected. However, the conclusions obtained were also found to be valid when the analysis period of 1901–2010 was used.

2.2. Large ensemble atmospheric simulation (d4PDF)

In addition to the observational data sets, we used a set of large ensemble historical simulations for 1951–2010, which are referred to as the database for Policy Decision making for Future climate change (d4PDF; Mizuta et al. 2017). The d4PDF archive consists of 100 global simulation members obtained using the Meteorological Research Institute Atmospheric General Circulation Model (MRI-AGCM; Mizuta et al. 2012) version 3.2 (which provides a horizontal resolution of approximately 60 km) and 50 regional downscaling simulation members covering the area of Japan that were obtained using the Nonhydrostatic Regional Climate Model (MRI-NHRCM; Sasaki et al. 2011)(with a horizontal resolution of 20 km). These simulations were driven by the observed boundary conditions of monthly varying SST, sea ice concentration, and radiative forcing, and the ensemble was generated by perturbing SST in a range of observational uncertainties. The ensemble-mean anomalies therefore define the atmospheric response to changes in the boundary condition (with a particular focus on SST), whereas deviations from the ensemble mean are regarded as being related to the internal variability of the atmosphere, which can occur irrespective of SST and sea ice anomalies.

2.3. Definition of Multiyear La Niña

To detect La Niña events, we used a three-month running mean time series of observed SST anomalies averaged over the Niño 3.4 region (170°–120° W, 5° S–5° N), which is hereafter referred to as the Niño 3.4 index. Multiyear La Niña were then defined as occurring when the Nino 3.4 index was below -0.5 K for two consecutive winters (November–December–January, NDJ). We extracted ten events for the period 1901–2017 (1908, 1916, 1949, 1954, 1970, 1973, 1983, 1998, 2007, and 2010) and six events for the period 1951–2010 (Fig. 1). Three multiyear La Niña events that were counted during 1951–2010 persisted for three consecutive years (triple-year events). Single-year La Niña occurred as frequently as multiyear La Niña: eleven times during 1901–2017 and five times during 1951–2010. During 1951–2010, the occurrence of La Niña from the conventional view (NDJ mean Niño 3.4 index below -0.5 K) occupied 20 years, and 15 years of these were categorized as multiyear events (including triple-year events). In addition, five out of six multiyear La Niña events were accompanied by strong El Niño events occurring in the previous year, which suggests that the amplitude of El Niño controls the duration of subsequent La Niña events (Wu et al. 2019; DiNezio et al. 2017a; Okumura 2019). Our study identified the same multiyear La Niña events as Okumura et al. (2017), even though the SST data used and the definition of multiyear La Niña differ between the two studies.

The effects of multiyear La Niña on large-scale atmospheric circulation and SAT over Japan were investigated by making composite anomalies with respect to the first and second years of multiyear La Niña (denoted as Years 0 and 1, respectively). For example, midsummer (June–July–August) and late summer (August–September–October) periods that corresponded with the developing phase of La Niña in the first year were denoted as JJA(0) and ASO(0), respectively. Anomalies with respect to observations and reanalysis and d4PDF data were defined as deviations from the monthly climatology for 1981–2010. Before the analysis, the linear trends for the entire period were removed at each grid point.

3. Japan SAT anomalies associated with multiyear La Niña

In this section, we investigate the time evolution of Japan SAT anomalies during multiyear La Niña by taking the composite of anomalies for the years listed in Section 2.3. Prior to making a comparison, we first present the Japan SAT anomalies during all La Niña events to revisit the conventional view of the impact of La Niña on temperature over Japan. Figure 2 shows the observed composites of the Niño 3.4 index and temperature over Japan. The time evolution of the Japan SAT anomaly indicates that a significantly hot summer of +0.4 K peaked from July to September, and a cold winter with approximately the same magnitude as that of summer occurred from November to February (Fig. 2a). The spatial distribution of SAT anomalies obtained at 13 stations and four sectors (Section 2.1) is nearly uniform and covers the whole of Japan (Fig. 2b–d). These composites confirm that Japan tends to experience hotter summers and colder winters than the climatological mean during La Niña events.

3.1. Temporal evolution

The peak of multiyear La Niña occurs in the NDJ of both Years 0 and 1, with Niño 3.4 SST anomaly of -1.3 and -1.0 K, respectively (shading in Fig. 3a). There is a decrease in the Niño 3.4 SST anomaly during the summer season of Year 1, but it remains negative, which indicates that La Niña persists beyond the conventional decay phase of the ENSO cycle. The composite SAT anomalies over Japan show a time evolution that is similar to that of the conventional case (Fig. 2a) in Years 0 and 1; positive in summer and negative in winter, corresponding to the anomalous hot summer and cold winter. However, a careful comparison of the maximum SAT anomaly during the two years indicates that the high temperature occurs in late summer (ASO) in Year 0 and in the midsummer (JJA) in Year 1 (Fig. 3a). Although the SAT anomalies are not statistically significant for 1951–2010 (Fig. 3a), they are significant at the 95% level during the summers for 1901–2017 (Fig. 3b). Interestingly, La Niña reaches its maximum during the winter season, but the SAT anomalies over Japan are statistically significant only during summer for 1951–2010; this is perhaps due to the large amplitude of noise during the winter, which masks the SST-driven signal. Therefore, the sample size for the observed composites may be too small to detect the SAT anomaly in response to La Niña events. When a similar composite analysis is applied to the d4PDF ensemble, both the anomalous hot summer and cold winter can be detected at the 99% significance level (Fig. 3c), and the model also captures the difference in the peak period of the hot summer signal in Years 0 and 1.

3.2. Spatial pattern

Figure 4 shows the observed composite SAT anomalies over Japan during multiyear La Niña. The anomalous hot summer in Year 0 occurs in ASO but not in JJA mainly over the western half of Japan (Fig. 4a, b); however, in Year 1, the anomalous hot condition is found only in JJA over the northern part (Fig. 4d, e). These anomalies are significant at the 95% level in the station data, and the difference in the peak period between the two years is consistent with the information presented in Fig. 3a. As the anomalous cold condition (Fig. 4c) seen during the mature phase of the first winter (i.e., DJF(0/1)) is not significant, the subsequent sections of this paper focus on the influence of multiyear La Niña on the summer temperature over Japan and the associated circulation anomalies.

The composite analysis of SAT anomalies obtained from the d4PDF regional downscaling simulations by the MRI-NHRCM revealed the spatial structure over Japan and the surrounding areas (Fig. 5). Analogous to the observations, an anomalous hot condition occurred over the western side of Japan in ASO of Year 0 (Fig. 5b), but over the northern side in JJA of Year 1 (Fig. 5c). The positive SAT anomaly in ASO of Year 0 is centered over the subtropics to the east of Taiwan, but it is weak and does not expand northward in JJA(0). The positive SAT anomaly in JJA of Year 1 is stronger than that in Year 0, and it extends from the east of Japan where it remains until ASO(1). These simulation patterns suggest that Japan SAT anomalies occur as a part of the large-scale circulation change and are not due to local processes.

4. Large-Scale atmospheric response to multiyear La Niña

4.1. Atmospheric circulation pattern

To understand the La Niña teleconnection that gives rise to an abnormally hot summer over Japan, we first compared atmospheric circulation anomalies between Year 0 and 1. The composite maps of anomalous temperature and horizontal winds at 850 hPa in JJA and ASO obtained from the CERA-20C reanalysis are shown in Fig. 6. In JJA(0) and ASO(0), the positive temperature anomaly is found around the western Pacific and South China Sea while the negative temperature anomaly appears around Japan only in JJA(0) (Fig. 6a). As shown in the observations (Fig 3), negative temperature anomalies around Japan tend to be obscure with increased number of samples in JJA(0). In ASO(0), significant warming associated with the anomalous southerly winds extends from the tropics to the coasts of East Asia, including the western part of Japan (Fig. 6b). During Year 1, the positive temperature anomaly covers northern part of Japan in JJA(1), but not in ASO(1) (Fig. 6c, d). In ASO(1), Southerly wind anomalies can only reach Taiwan inhibited by westerly wind anomaly.

Some of the composite anomalies in the CERA-20C reanalysis are not statistically significant at the 95% level, and this is probably due to the small sample size. However, it is possible to reproduce the important part of the observed anomalies with a sufficient statistical significance in the d4PDF-GCM simulation, which employs a sample size that is 100 times larger than that of CERA-20C (Fig. 7). The d4PDF-GCM shows positive 850 hPa temperature anomalies over the South China Sea in Year 0, which are accompanied by southerly wind anomalies (Fig. 7a, b). Analogous to the reanalysis data, the warming extends northward to cover western Japan only in ASO(0), which is consistent with the composite SAT anomaly patterns (Fig. 5a, b). In JJA(1), the temperature anomalies are negative in the tropics, opposite to JJA(0), and the anticyclonic circulation anomaly is absent over the tropical western North Pacific (TWNP) (Fig. 7c). A patch of positive temperature anomalies zonally extend from northern Japan to the North Pacific in JJA(1), but these are not likely to couple with the low-level circulation anomalies in the tropics. In ASO(1), the anticyclonic circulation anomaly forms as in ASO(0), but the southerly wind anomalies are very weak (Fig. 7d).

The contrast between the anomalous atmospheric states in Years 0 and 1 with respect to the coupling between the tropics and midlatitudes around Japan is similarly seen in the 500 hPa geopotential height (Z500) composites in CERA-20C and d4PDF-GCM (Fig. 8). The composite maps in the CERA-20C reanalysis show significant high-pressure anomalies around the tropical north western Pacific in JJA(0). A low-pressure anomaly exists to the east of Japan, and this apparently corresponds to the low-level cooling beneath (Fig 6a).

In Year 1, a high-pressure anomaly over the North Pacific encompasses northern Japan in CERA-20C and d4PDF (Fig. 8c, g). This positive Z500 anomaly was also identified by Maeda (2014), who analyzed the midsummer Z500 pattern correlated with the ENSO monitoring index in JMA. Positive geopotential height anomalies that are similar to those of Z500 are identified at the lower and upper troposphere, indicating a quasi-barotropic structure (not shown). Consequently, it is plausible that the barotropic high-pressure anomaly can increase the SAT over Japan via adiabatic warming. In ASO, a high-pressure signal appears only over the North Pacific around the date line (Fig. 8f, h), but it has little effect on the temperature enveloping Japan.

4.2. SST and precipitation patterns

In the previous section, we analyzed the large-scale atmospheric anomalies occurring during multiyear La Niña. To understand the forcing mechanism, we investigated the composites of the observed anomalies in SST and precipitation (Fig. 9). The amplitudes of La Niña SST anomalies are similar in both Years 0 and 1 in JJA but they differ in ASO (see Fig. 9, bottom right), and the SST anomaly is approximately 25% larger in Year 0 (generally, La Niña has a stronger peak in the first year). In general, the SST anomaly patterns share the common structure of La Niña in both years: cooling in the central-eastern equatorial Pacific and warming around the Maritime Continent. However, the Indian Ocean is slightly warmer than the climatology in Year 0 and colder in Year 1. This difference can be explained by the fact that most of the multiyear La Niña events follow El Niño in the previous year (Fig. 2), which can lead to delayed Indian Ocean warming (known as the Indian Ocean Capacitor effect; Xie et al. 2009) in Year 0. The other difference is the meridional width of the negative SST anomalies in the central-eastern Pacific; these are narrow in Year 0 and wide in Year 1.

As with SST, precipitation anomaly patterns are similar in both years: there is an increase in precipitation over the Maritime Continent and a decrease to the east extending along the Pacific Intertropical Convergence Zone (ITCZ). A closer look at the anomaly patterns in the western Pacific shows that a significant decrease in precipitation occurs in the TWNP in JJA(0) (Fig. 9a). This large negative precipitation anomaly could occur in response to the Indian Ocean warming, which induces a subsidence anomaly to the northeast (Xie et al. 2009, 2016). In contrast to Year 0, the negative precipitation anomaly around the TWNP is not found in JJA(1), which is consistent with the absence of the Indian Ocean warming (Fig. 9c). Furthermore, SST and precipitation signals in ASO(1) are weak (Fig. 9d). The d4PDF can reproduce the interannual variability of the precipitation response accompanied by ENSO (Kamae et al. 2017). In fact, the anomalous pattern of precipitation associated with multiyear La Niña is to a large extent consistent with observations (not shown).

From the composite anomalies of large-scale atmospheric states, SST, and precipitation, we hypothesize the existence of two different mechanisms that cause hot summers over Japan in different seasons during multiyear La Niña, as follows: the late summer warming in Year 0 is caused by warm temperature advection associated with the low-level anticyclonic circulation anomaly over the TWNP, and the midsummer warming in Year 1 is explained by the extension of adiabatic warming to northern Japan through large-scale high-pressure anomalies with a barotropic structure over the North Pacific. Given that precipitation anomalies measure diabatic heating anomalies to force the circulation response, it is a little puzzling that tropical precipitation anomaly patterns are similar in both years. We thus hypothesize that the subtle differences between them are important for exciting the different teleconnection pathways.

5. Diagnosing teleconnection mechanisms

As previously mentioned, it is possible to explain the different teleconnection pathways in Years 0 and 1 (Section 4.1) by the different atmospheric circulation responses to diabatic heating anomalies associated with multiyear La Niña. To verify the mechanisms behind the hot summer over Japan, we used the linear baroclinic model (LBM; Watanabe and Kimoto 2000), which calculates a steady linear response in the atmosphere to a prescribed thermal forcing. As the vertical integral of thermal forcing is equivalent to the precipitation anomalies presented in Section 4.2 (assuming radiative heating anomalies are not important in the present problem), we constructed four patterns of idealized thermal forcing based on the composite anomalies of observed precipitation (Fig. 10). To mimic the typical condensational heating structure relating to deep convection, the vertical structure of the thermal forcing was assumed to have a peak in the middle of the troposphere at around 500 hPa. Furthermore, the seasonal mean basic states (vorticity, divergence, temperature, and surface pressure) were adopted from the CERA-20C climatology.

For simplicity, the anomalous heating over the Maritime Continents (denoted as MC heating) was identical in the four sets of the forcing. In Year 0, the anomalous cooling over the eastern Pacific (EP cooling) was the same in JJA(0) and ASO(0), but an additional strong cooling was prescribed in JJA(0) over the tropical western North Pacific (TWNP cooling), whereas cooling over the equatorial western Pacific (WP cooling) was prescribed in ASO(0) (Fig. 10a, b). In Year 1, a pair of MC heating and WP cooling was prescribed, with the latter slightly stronger in JJA(1) than in ASO(1). We ignored EP cooling in Year 1 because the precipitation anomaly is weak (Fig. 9c, d). There was no change to our conclusion when weak EP cooling was included in Year 1.

Figure 11 shows the steady responses of 850 hPa temperature and winds in Year 0. For the different forcing patterns shown in Figs. 10a, b with different basic states, a clear difference can be seen between the steady responses in JJA(0) and ASO(0). The 850 hPa temperature response around Japan is weak in JJA(0) but strong and positive in ASO(0), and the latter is probably due to a southwesterly wind response (Fig. 11a, b). These contrasts between the steady responses in JJA(0) and ASO(0) are mostly consistent with the composite anomaly patterns in the reanalysis and d4PDF (Figs. 6 and 7). A close comparison shows that the LBM has a false warm signal centered in North Japan in ASO(0), while reanalysis reveals the warm anomaly located over the East China Sea. This discrepancy may arise from the Z500 response around North Japan being too strong in the LBM.

The contribution from regional heating and cooling given to the LBM for the temperature response over Japan in Year 0 was then evaluated by repeating the calculation with each of the MC, TWNP, WP, and EP thermal forcing (Fig. 11c). We did not provide thermal forcing around Japan, therefore, in our model, the temperature response around Japan is caused solely by adiabatic processes. JJA responses are weaker than those of ASO for all regional forcings, which implies that the difference in the basic state plays a role. In both seasons, EP cooling contributes to warming over Japan, whereas MC heating has negligible contribution to the temperature response around Japan. A notable difference is the response to TWNP cooling in JJA(0) and WP cooling in ASO(0). TWNP cooling causes a meridional tripolar pattern in the temperature field, which is akin to the well-known Pacific–Japan teleconnection (Nitta 1987, 1990): positive around the TWNP, negative over Japan, and positive over northern Japan (not shown), whereas WP cooling drives a large-scale anticyclonic circulation in the lower troposphere via the Matsuno–Gill response (Matsuno 1966; Gill 1980) and brings warm advection from the tropics to the southwestern part of Japan. Consequently, the temperature signal is weak in JJA(0) but strongly positive in ASO(0).

The mechanism involved in causing the hot summer in JJA(1) was analyzed using the LBM experiment (Fig. 12). The 850 hPa temperature response shows that northern Japan is covered by a warm signal. (Fig. 12a). Although a high temperature signal can be found over northern Japan and northeastern China in CERA-20C, the LBM shows only the North Pacific, probably due to the weak temperature magnitude bias near the surface in the LBM. However, as the anticyclonic circulation response around the TWNP is weak and detached from the warming over Japan, it is unlikely that the mechanism can be explained by the lower tropospheric circulation response, unlike in Year 0. Instead, the LBM reproduces a barotropic high-pressure response at 500 hPa (Fig. 12b). Consistent with the Z500 anomaly pattern in d4PDF (Fig. 8g), the anomalous high extends from northern Japan to the North Pacific near the date line. As shown in Fig. 11c, we diagnosed the relative contribution of the regional thermal forcing to the Z500 response over the rectangular region in Fig. 12b (figure not shown). For the total Z500 response, the contribution from the MC heating and the WP cooling works opposite sign; the former is weakly negative, but the latter is strongly positive. Consequently, the diabatic cooling over the western Pacific associated with the decrease in precipitation (Fig. 9c) dominates with respect to exciting the barotropic wave response to the north and is thus responsible for the hot summer over Japan in Year 1.

In summary, the mechanisms behind the two teleconnection types responsible for the hot summers over Japan during multiyear La Niña have been verified using the steady linear response to idealized thermal forcing, which mimicked the observed precipitation anomalies. In ASO(0), diabatic cooling in the western Pacific excites the lower tropospheric circulation responsible for an anomalous southerly advection that warms Japan. This mechanism does not operate in JJA(0) for two reasons: the amplitude of the response is different because of the difference in the basic state, and diabatic cooling is located in a different area (around the TWNP in JJA(0)). In JJA of Year 1, a barotropic high-pressure response is forced by diabatic cooling in the equatorial western Pacific.

6. Summary and discussion

This study investigated the multiyear La Niña impacts on the temperature over Japan in summer based on observations, reanalysis data, and large ensemble historical simulations conducted using AGCM and regional climate model. The multiyear La Niña, which lasts for two years, occurs frequently and accounts for approximately 70% of the total La Niña events. It has been argued that conventional La Niña causes a hotter summer than usual over Japan, as does multiyear La Niña. However, we showed that the hot summer period and the associated area in which it occurs differ between the first and second years when La Niña persists for two years. During the first summer (Year 0), the southwestern part of Japan tend to be hot in late summer (August to October), whereas during the second summer (Year 1) northeastern Japan experiences the hot condition in the middle of summer (June to August). These features are robust in all data sets and also captured by the large ensemble simulations.

The mechanisms involved in these two types of teleconnection that induce hot summers over Japan are summarized in Fig. 13a, b. The late summer warming over western Japan in Year 0 occurs as a part of the lower tropospheric circulation change over the TWNP, which causes warm temperature advection from the tropics. The midsummer warming in Year 1 is accompanied by a barotropic high-pressure anomaly over the North Pacific extending to northern Japan. These circulation anomalies can be obtained as a steady linear response to the anomalous heating/cooling associated with multiyear La Niña.

The seasonal differences between the two teleconnection types and their relationship to temperature over Japan is shown in Fig. 13c. The hot summer mechanism does not work in JJA of Year 0 because the atmospheric responses to the anomalous cooling around the TWNP and the equatorial central–eastern Pacific are canceled each other (Fig. 11c). The diabatic cooling around the TWNP is associated with decrease precipitation, and it induces a meridional tri-pole in the temperature field that includes cooling over Japan. This response pattern is reminiscent of the PJ teleconnection, which is observed when an extreme summer occurs over Japan (Nitta 1987, 1990). There is a possibility that a strong El Niño preceding a Year 0 La Niña causes delayed Indian Ocean warming, which then excites the PJ pattern acting to cool summer in Japan (Xie et al. 2009, 2016; Kosaka et al. 2013). This effect counteracts the warming directly induced by the convective anomaly in the equatorial Pacific, and the Japan SAT anomaly becomes insignificant in JJA of Year 0. As the Indian Ocean warming effect measured by the precipitation around the TWNP disappears after JJA(0), a hot summer tends to appear over Japan in ASO(0). This result represents a possibility that summer temperature anomalies over Japan from El Niño to La Niña transition phase can be interpreted as a linear combination of the atmospheric responses to a decaying El Niño and a developing La Niña in summer.

In the second year of multiyear La Niña (Year 1), weak negative SST anomalies occur in the Indian Ocean due to the delayed effect of the first year La Niña (Fig. 9c, d). However, significant precipitation anomalies are absent over the northern Indian Ocean and the TWNP in Year 1. Instead, the warm temperature anomalies over Japan seen in JJA of Year 1 (Figs. 4d and 5c) are probably associated with barotropic height anomalies over the North Pacific extending to Japan. During ASO, the high-pressure anomaly is located over the North Pacific near the date line, but it does not extend westward. There is a possibility that the summertime basic state (in particular, the weak Asian jet) causes different stationary Rossby wave response patterns to the equatorial forcing in the two seasons.

Unlike previous analyses, which have shown the teleconnection associated with conventional La Niña, we observed distinct seasonality and different spatial patterns of anomalous atmospheric states during multiyear La Niña. Since multiyear La Niña occurs as frequently as the single-year La Niña event, the conventional view of the La Niña impact may be a mixture of the two teleconnections seen in Years 0 and 1 of multiyear La Niña. Additional analysis implies that single-year La Niña also induces two type hot summer mechanisms in Japan (Fig. S1). We consider that there is no critical differences between Year 1 multiyear La Niña and Year 0 single-year La Niña impact on summer temperature over Japan (see also Supplements).

Multiyear La Niña is representative of one of the higher-order characteristics of ENSO in nature. Recent studies have shown that multiyear La Niña may have a longer predictability than conventional La Niña (DiNezio et al. 2017a,b) although the reason for the long predictability is not well understood. Further studies focusing on the mechanisms and predictability of multiyear La Niña will thus be beneficial for improving seasonal prediction skill over Japan.

Supplements

Supplement 1 provides the analysis of single-year La Niña impact on East Asia region and comparison with multiyear La Niña.

Acknowledgments

We acknowledge the modeling group for making the d4PDF data set available. We thank Youichi Kamae and two anonymous reviewers for their constructive comments to improve the manuscript. We also wish to thank Masahide Kimoto and Masaki Sato for their helpful comments. This work was supported by the Grant-in-Aid 26247079 and the Integrated Research Program for Advancing Climate Models from the Ministry of Education, Culture, Sports, Science, and Technology (MEXT), Japan.

References

An, S.-I., and J.-W. Kim, 2018: ENSO transition asymmetry: Internal and external causes and intermodel diversity. *Geophys. Res. Lett.*, **45**, 5095–5104.

Battisti, D. S., and A. C. Hirst, 1989: Interannual variability in a tropical atmosphere-ocean model: Influence of the basic state, ocean geometry and nonlinearity. *J. Atmospheric Sci.*, **46**, 1687–1712.

Chen, M., P. Xie, J. E. Janowiak, and P. A. Arkin, 2002: Global land precipitation: A 50-yr monthly analysis based on gauge observations. *J. Hydrometeorol.*, **3**, 18.

Chiang, J. C. H., and A. H. Sobel, 2002: Tropical tropospheric temperature variations caused by ENSO and their influence on the remote tropical climate. *J. Clim.*, **15**, 2616–2631.

Compo, G. P., J. S. Whitaker, and P. D. Sardeshmukh, 2006: Feasibility of a 100-year reanalysis using only surface pressure data. *Bull. Am. Meteorol. Soc.*, **87**, 175–190.

DiNezio, P. N., and C. Deser, 2014: Nonlinear controls on the persistence of La Niña. *J. Clim.*, **27**, 7335–7355.

——, and Coauthors, 2017a: A 2 year forecast for a 60-80% chance of La Niña in 2017-2018. *Geophys. Res. Lett.*, **44**, 11,624-11,635.

——, C. Deser, Y. Okumura, and A. Karspeck, 2017b: Predictability of 2-year La Niña events in a coupled general circulation model. *Clim. Dyn.*, **49**, 4237–4261.

Gill, A. E., 1980: Some simple solutions for heat-induced tropical circulation. *Q. J. R. Meteorol. Soc.*, **106**, 447–462.

Hirahara, S., M. Ishii, and Y. Fukuda, 2014: Centennial-scale sea surface temperature analysis and Its uncertainty. *J. Clim.*, **27**, 57–75.

Horel, J., and J. Wallace, 1981: Planetary-scale atmospheric phenomena associated with the southern oscillation. *Mon. Weather Rev.*,**109**, 831–829.

Hoskins, B. J., and D. Karoly, 1981: The steady linear response of a spherical atmosphere to thermal and orographic forcing. *J. Atmospheric Sci.*, **38**, 1179–1196.

Hu, Z.-Z., A. Kumar, Y. Xue, and B. Jha, 2014: Why were some La Niñas followed by another La Niña? *Clim. Dyn.*, **42**, 1029–1042.

Jin, F.-F., 1997: An equatorial ocean recharge paradigm for ENSO. Part I: conceptual model. *J. Atmospheric Sci.*, **54**, 811–829.

——, J. D. Neelin, and M. Ghil, 1994: El Nino on the devil's staircase: annual subharmonic steps to chaos. *Science*, **264**, 70–72.

JMA, 2017: Climate change monitoring report 2017. *JMA*, 93 (In Japanese).

Kalnay, E., and Coauthors, 1996: The NCEP/NCAR 40-year reanalysis project. *Bull. Am. Meteorol. Soc.*, **77**, 437–471.

Kamae, Y., W. Mei, S.-P. Xie, M. Naoi, and H. Ueda, 2017: Atmospheric Rivers over the Northwestern Pacific: Climatology and interannual variability. *J. Clim.*, **30**, 5605–5619.

Kitoh, A., 1988: Correlation between the surface air temperature over Japan and the global sea surface temperature. *J. Meteorol. Soc. Jpn.*, **66**, 967–986.

Klein, S. A., B. J. Soden, and N.-C. Lau, 1999: Remote Sea Surface Temperature Variations during ENSO: Evidence for a Tropical Atmospheric Bridge. *J. Clim.*, **12**, 917–932.

Kosaka, Y., S.-P. Xie, N.-C. Lau, and G. A. Vecchi, 2013: Origin of seasonal predictability for summer climate over the Northwestern Pacific. *Proc. Natl. Acad. Sci.*, **110**, 7574–7579.

Kurihara, K., 1985: Relationship between the surface air temperature in Japan and sea water temperature in the western tropical Pacific during summer. *Tenki*, 407–417 (In Japanese).

Laloyaux, P., and Coauthors, 2018: CERA-20C: A coupled reanalysis of the twentieth century. *J. Adv. Model. Earth Syst.*, **10**, 1172–1195.

Lau, N.-C., 1997: Interactions between global SST anomalies and the midlatitude atmospheric circulation. *Bull. Am. Meteorol. Soc.*, **78**, 21–33.

Luo, J.-J., G. Liu, H. Hendon, O. Alves, and T. Yamagata, 2017: Inter-basin sources for two-year predictability of the multi-year La Niña event in 2010–2012. *Sci. Rep.*, **7**.

Maeda, S., 2014: ENSO and Japan's climate. *Meteorol. Res. Note*, 167–179 (In Japanese).

Matsuno, T., 1966: Quasi-geostrophic motions in the equatorial area. *J. Meteorol. Soc. Jpn. Ser II*, **44**, 25–43.

Miyazaki, Y., 1989: Japan weather characteristics on El Niño year. *Tenki*, **15**, 489–498 (In Japanese).

Mizuta, R., and Coauthors, 2012: Climate Simulations Using MRI-AGCM3.2 with 20-km Grid. *J. Meteorol. Soc. Jpn.*, **90A**, 233–258, https://doi.org/10.2151/jmsj.2012-A12.

Mizuta, R., and Coauthors, 2017: Over 5,000 years of ensemble future climate simulations by 60-km global and 20-km regional atmospheric models. *Bull. Am. Meteorol. Soc.*, **98**, 1383–1398.

Nitta, T., 1987: Convective activities in the tropical western Pacific and their Impact on the northern hemisphere summer circulation. *J. Meteorol. Soc. Jpn. Ser II*, **65**, 373–390.

——, 1990: Unusual summer weather over Japan in 1988 and its relationship to the tropics. *J. Meteorol. Soc. Jpn.*, **68**, 575–588.

Okumura, Y. M., 2019: ENSO Diversity from an Atmospheric Perspective. *Curr. Clim. Change Rep.*, **5**, 245–257.

——, and C. Deser, 2010: Asymmetry in the duration of El Niño and La Niña. *J. Clim.*, **23**, 5826–5843.

——, P. DiNezio, and C. Deser, 2017: Evolving impacts of multiyear La Niña events on atmospheric circulation and U.S. drought: Evolving impacts of multiyear La Niña. *Geophys. Res. Lett.*, **44**, 11,614-11,623.

Poli, P., and Coauthors, 2016: ERA-20C: An atmospheric reanalysis of the twentieth century. *J. Clim.*, **29**, 4083–4097.

Sasaki, H., A. Murata, M. Hanafusa, M. Oh'izumi, and K. Kurihara, 2011: Reproducibility of Present Climate in a Non-Hydrostatic Regional Climate Model Nested within an Atmosphere General Circulation Model. *SOLA*, **7**, 173–176, https://doi.org/10.2151/sola.2011-044.

Schott, F. A., S.-P. Xie, and J. P. McCreary, 2009: Indian Ocean circulation and climate variability. *Rev. Geophys.*, **47**, 46.

Sobel, A. H., I. M. Held, and C. S. Bretherton, 2002: The ENSO signal in tropical tropospheric temperature. *J. Clim.*, **15**, 2702-2706.

Tanaka, M., M. Takekawa, and S. Notsuharu, 2015: Characteristics of Japan climate during El Niño and La Niña event. *Train. Text Seas. Forecast*, **27**, 152–163 (In Japanese).

Trenberth, K. E., 2002: Evolution of El Niño–Southern Oscillation and global atmospheric surface temperatures. *J. Geophys. Res.*, **107**, 13.

——, G. W. Branstator, D. Karoly, A. Kumar, N.-C. Lau, and C. Ropelewski, 1998: Progress during TOGA in understanding and modeling global teleconnections associated with tropical sea surface temperatures. *J. Geophys. Res. Oceans*, **103**, 14291–14324.

Tziperman, E., L. Stone, M. A. Cane, and H. Jarosh, 1994: El Niflo chaos: Overlapping of resonances between the seasonal cycle and the Pacific ocean-atmosphere oscillator. *Science*, **264**, 72–74.

Wallace, J., and D. Gutzler, 1981: Teleconnections in the geopotential height field during the Northern hemisphere winter. *Mon. Weather Rev.*, **109**, 784–912.

Watanabe, M., and M. Kimoto, 2000: Atmosphere-ocean thermal coupling in the North Atlantic: A positive feedback. *Q. J. R. Meteorol. Soc.*, **126**, 3343–3369.

Wu, X., Y. M. Okumura, and P. N. DiNezio, 2019: What controls the duration of El Niño and La Niña events? *J. Clim.*, **32**, 5941–5965.

Xie, S.-P., K. Hu, J. Hafner, H. Tokinaga, Y. Du, G. Huang, and T. Sampe, 2009: Indian Ocean capacitor effect on Indo–Western Pacific climate during the summer following El Niño. *J. Clim.*, **22**, 730–747.

——, Y. Kosaka, Y. Du, K. Hu, J. S. Chowdary, and G. Huang, 2016: Indo-western Pacific ocean capacitor and coherent climate anomalies in post-

ENSO summer: A review. *Adv. Atmospheric Sci.*, **33**, 411–432.

Yulaeva, E., and J. Wallace, 1994: The signatre of ENSO in global temperature and precipitation fields derived from the microwve sounding unit. *J. Clim.*, **7**, 1719–1736.

List of Figures

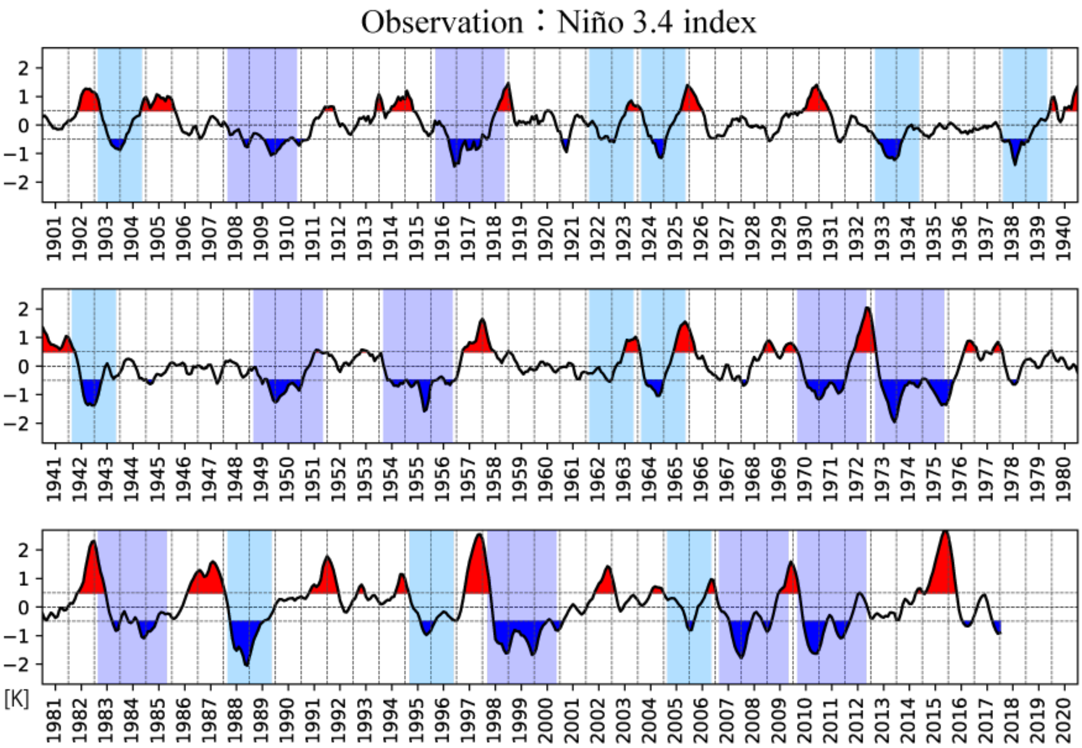

Fig. 1 Time series of the observed Niño 3.4 index. Red and blue colors show the anomaly above 0.5 K and below -0.5 K, respectively, corresponding to El Niño and La Niña. Years shaded in purple represent multiyear La Niña events and those in light-blue represent single-year La Niña events.

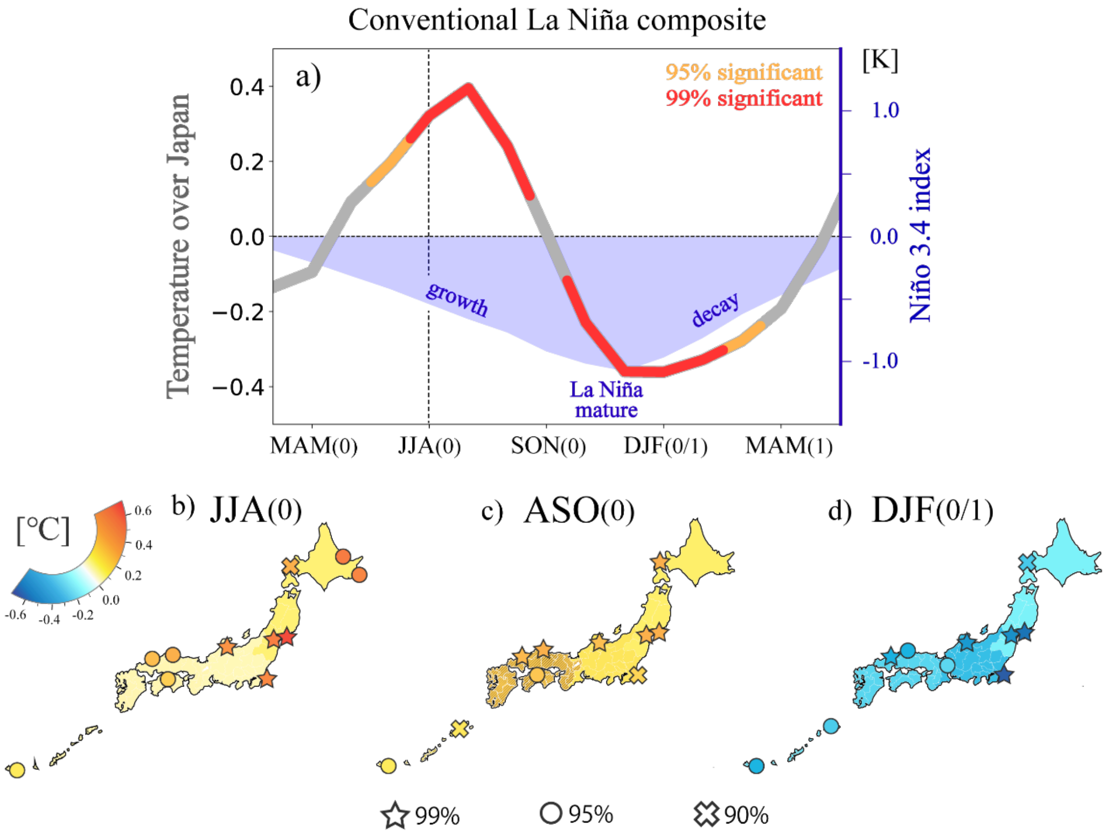

Fig. 2 (a) Composite of the Niño 3.4 index (shading) and Japan SAT anomaly (curve) for all La Niña events during 1901–2017 (35 events) obtained from COBE-SST2 and JMA SAT data. Statistically significant SAT anomalies at the 95% and 99% levels are shown in orange and red. (b) Spatial distribution of composite SAT anomalies for four sectors over Japan for all La Niña events during 1951–2010 (20 events) in JJA(0), ASO(0), and DJF(0/1), where an anomaly significant at the 95% level is shown by the hatching. The SAT anomalies at weather stations are shown by symbols (crosses, circles, and stars) representing those significant at the 90%, 95%, and 99% levels, respectively.

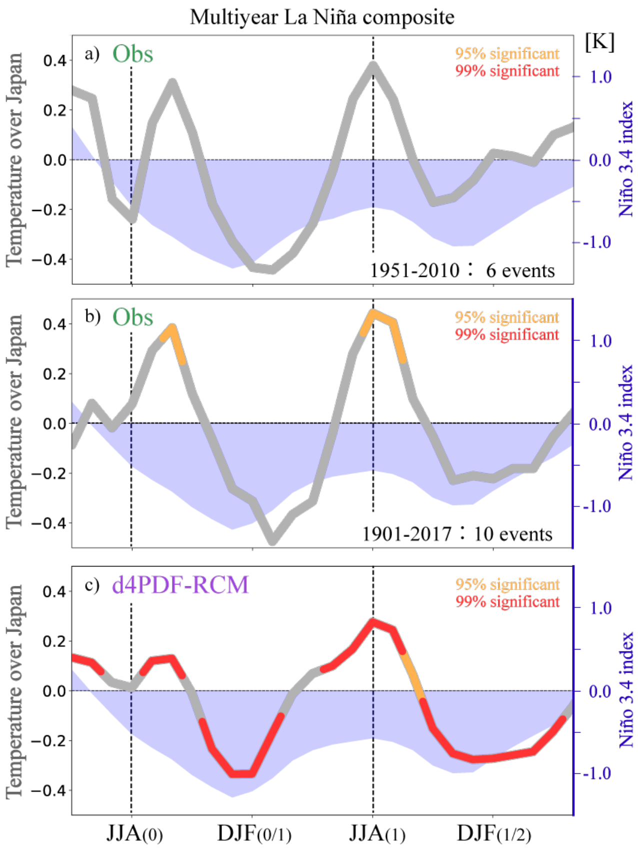

Fig. 3 As in Fig. 2a, but for multiyear La Niña events during (a) 1951–2010 and (b) 1901–2017. The number of multiyear La Niña events for each period is shown in the bottom right corner. (c) As in (a), but for the composite from d4PDF regional downscaling data.

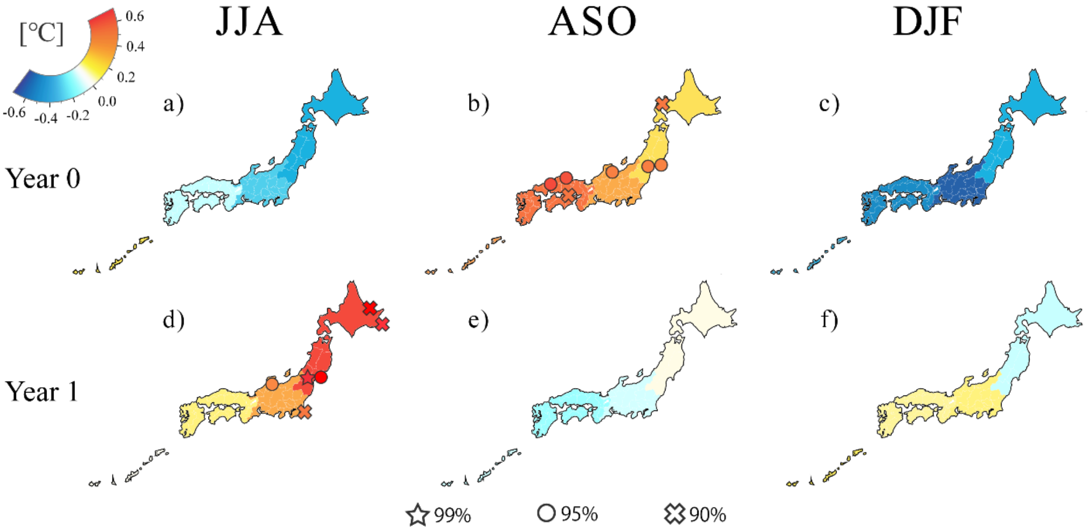

Fig. 4 As in Fig. 2b, but for multiyear La Niña events: (a) JJA(0), (b) ASO(0), (c) DJF(0/1), (d) JJA(1), (e) ASO(1), and (f) DJF(1/2).

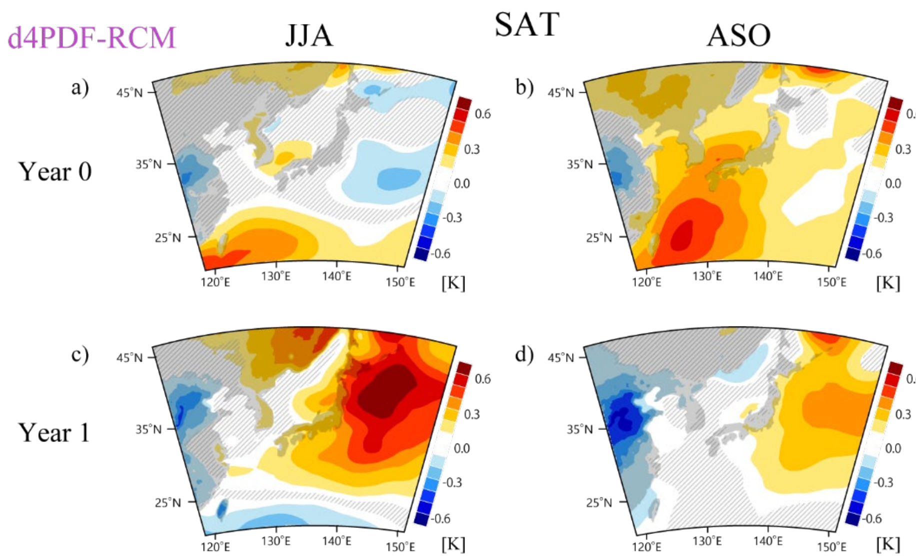

Fig. 5 Multiyear La Niña composite of SAT anomaly from the d4PDF regional downscaling simulations: (a) JJA(0), (b) ASO(0), (c) JJA(1), and (d) ASO(1). Anomalies not significant at the 95% level are shown by the hatching.

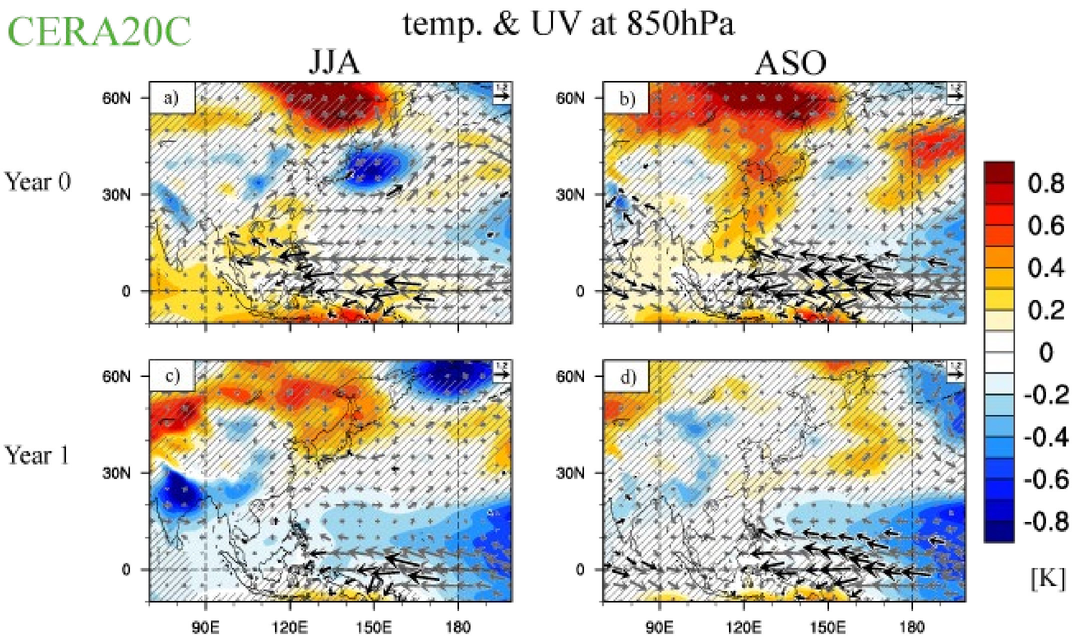

Fig. 6 Multiyear La Niña composite of temperature (shading) and horizontal winds (vector; unit is m s^{-1}) at 850 hPa from CERA-20C: (a) JJA(0), (b) ASO(0), (c) JJA(1), and ASO(1). Hatched areas and gray vectors indicate anomalies that are not statistically significant at the 95% level. Black vectors are significant at the 95% level.

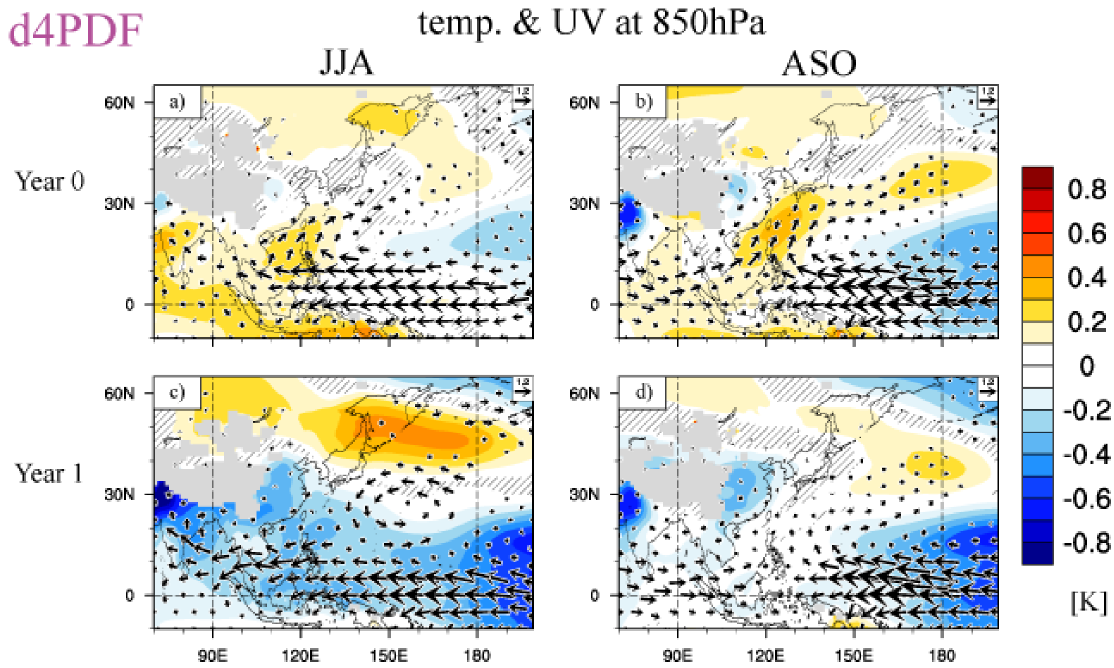

Fig. 7 As in Fig. 6, but for the d4PDF-GCM simulation. Wind anomalies significant at the 95% level are plotted.

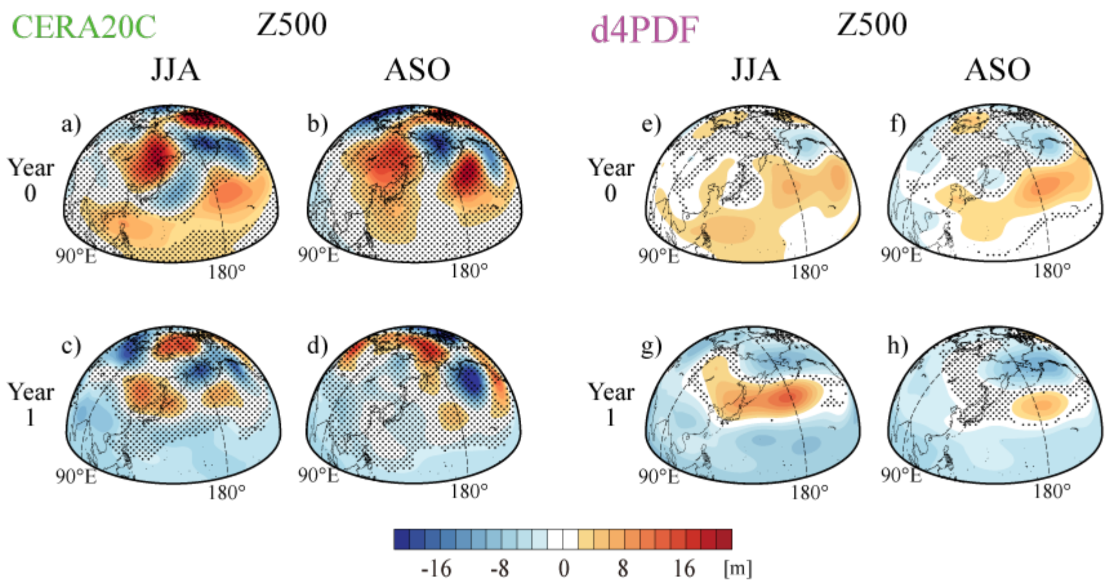

Fig. 8 Multiyear La Niña composite of 500 hPa geopotential height anomalies from CERA-20C: (a) JJA(0), (b) ASO(0), (c) JJA(1), and (d) ASO(1). Values not significant at the 95% level are represented by hatching. (e)–(h) As in (a)–(d) but for the d4PDF-GCM simulations.

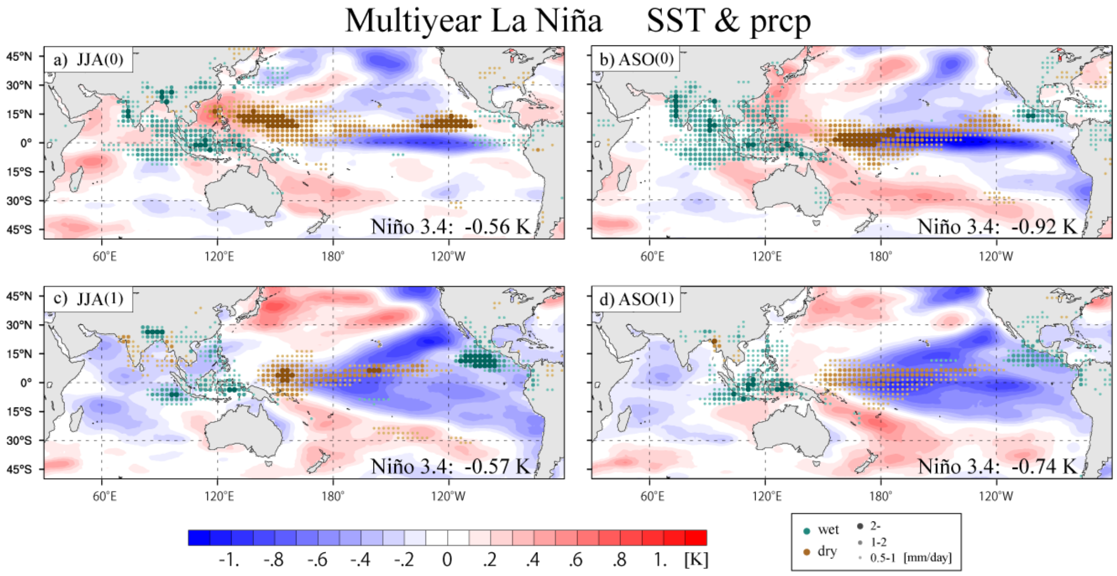

Fig. 9 Multiyear La Niña composite of anomalous SST (COBE-SST2; shading) and precipitation (PREC; dots): (a) JJA(0), (b) ASO(0), (c) JJA(1), and (d) ASO(1). Niño 3.4 SST anomaly values are shown in the bottom right corner.

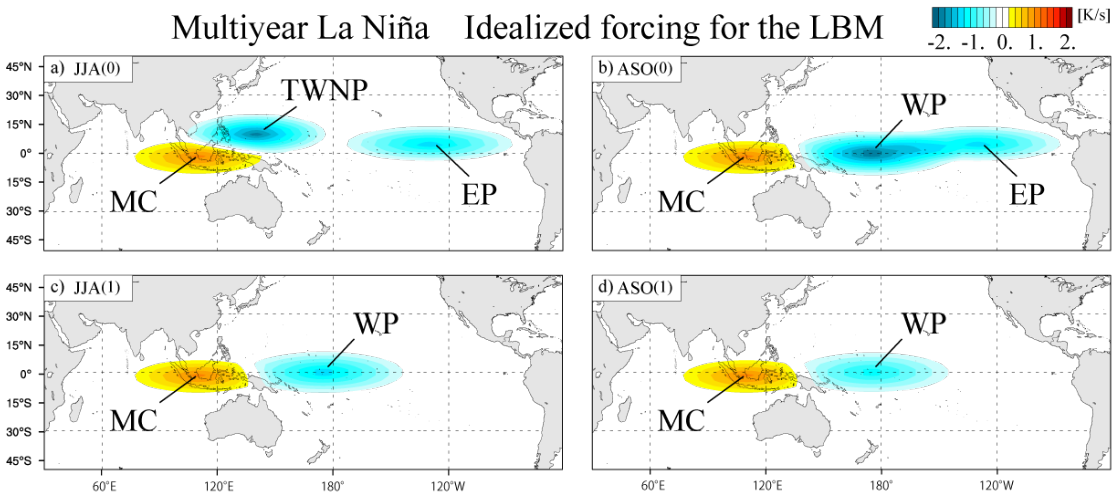

Fig. 10 Patterns of idealized diabatic heating and cooling for the LBM experiments: (a) JJA(0), (b) ASO(0), (c) JJA(1), and (d) ASO(1). The horizontal structure mimics the observed precipitation anomalies shown in Fig. 9. Heating and cooling occur over the Maritime Continent, tropical western North Pacific, western Pacific, and eastern Pacific, which are abbreviated as MC, TWNP, WP, and EP, respectively.

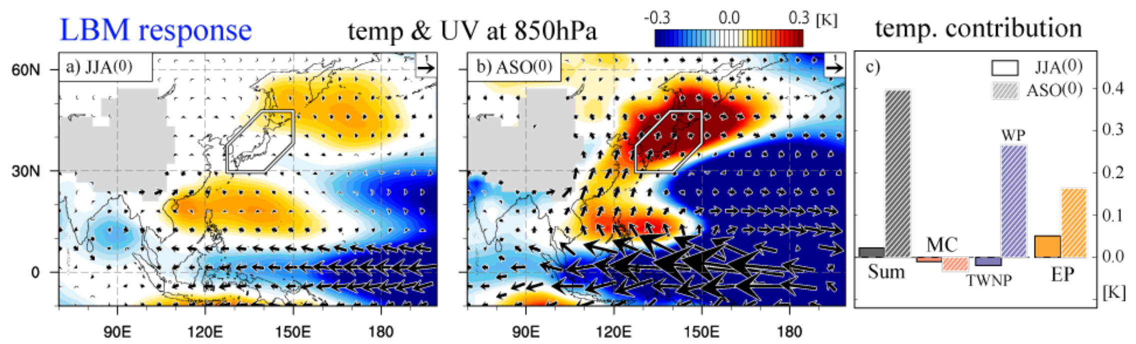

Fig. 11 As in Fig 6, but for the steady atmospheric response obtained from the LBM experiments for (a) JJA(0) and (b) ASO(0). Thermal forcing for the respective experiment is shown in Fig. 10a, b. The frame in (b) represents the region used to calculate the temperature response over Japan. (c) Contribution from individual forcings to the 850 hPa temperature response over Japan. Filled and hatched bars indicate JJA(0) and ASO(0), respectively. From the left to right, the bars indicate the sum, MC, TWNP (WP), and EP forcings in JJA(ASO).

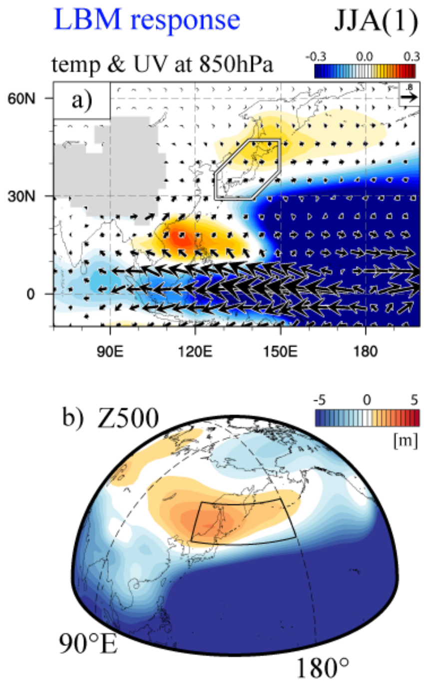

Fig. 12 Steady atmospheric response in (a) 850 hPa temperature and winds, and (b) Z500 in JJA(1) (thermal forcing is shown in Fig. 10c). The conventions used here follow those employed in Figs. 6c and 8c. The black rectangle in (b) represents the region used to measure the Z500 response around Japan.

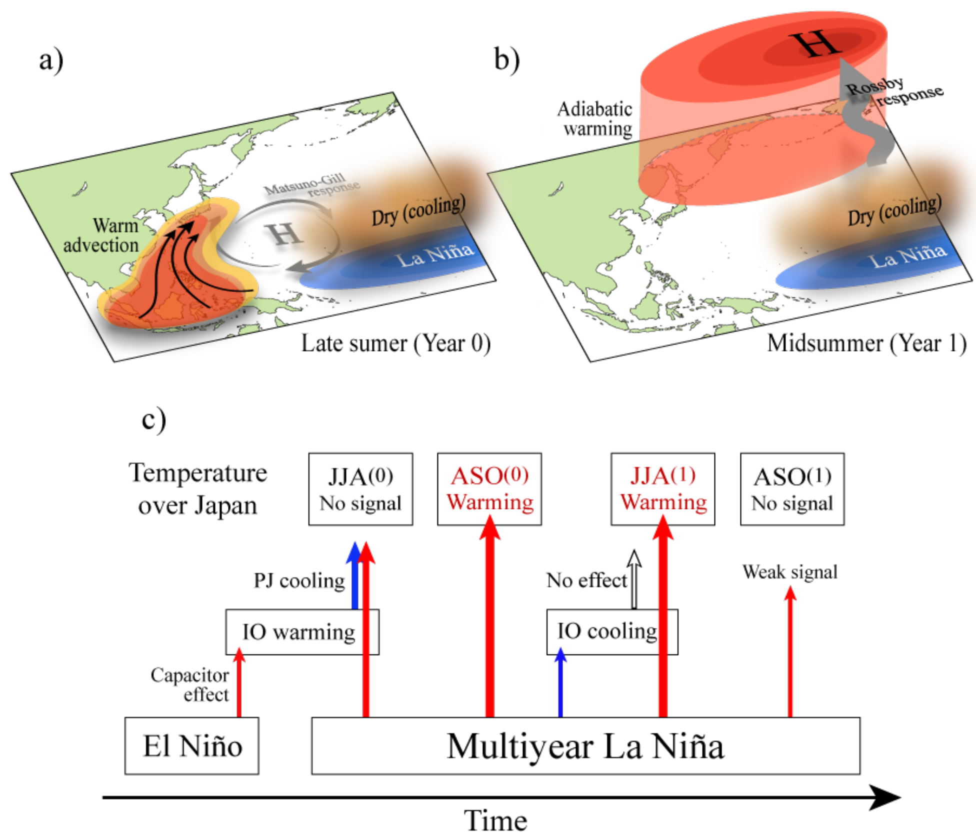

Fig. 13 Schematic illustrating multiyear La Niña impacts on the temperature over Japan during summer. (a)–(b) Distinct atmospheric teleconnection mechanism occurring during the first and second years, and (c) evolving impacts of multiyear La Niña and preceding El Niño on temperature over Japan. The red (blue) arrows indicate remote effects that warm (cool).